A new climatology of maximum and minimum temperature (1951-2010) in Spanish mainland: a comparison between three different interpolation methods

Journal:	*International Journal of Geographical Information Science*
Manuscript ID	IJGIS-2015-0479.R3
Manuscript Type:	Research Article
Keywords:	Climatology, Maximum Temperature, Minimum Temperature, Interpolation, Spain

A new climatology of maximum and minimum temperature (1951-2010) in the Spanish mainland: a comparison between three different interpolation methods

Abstract

This study presents a new climatology of monthly temperature for mainland Spain (1951-2010), performed with the highest quality and spatially dense, up-to-date monthly temperature data set available in the study area (MOTEDAS).

Three different interpolation techniques were evaluated: the Local Weighted Linear Regression (LWLR), the Regression-Kriging (RK) and the Regression-Kriging with stepwise selection (RKS), a modification of RK. The performances of the different models were evaluated by the leave-one-out validation procedure, comparing the results from the models with the original data and calculating different error measurements.

The three techniques performed better for Tmax than for Tmin, and for the cold, rather than warmer months; also at lower altitude than highland areas. The best results were achieved with LWLR applied for the first time on temperatures in the Spanish mainland. This method improved the accuracy of the temperature reconstruction with respect to RK and RKS.

We present a collection of Tmax and Tmin monthly charts, using the same temperature legend to prevent any visual bias in the interpretation of the results. The dataset is available upon request.

Key Words. Climatology; Interpolation; Maximum temperature; Minimum Temperature; Spain.

1. Introduction

Climatology maps express mean values of climate variables and are used as a working tool in several fields, such as agriculture, engineering, hydrology, ecology and natural resource management among others (Daly *et al.*, 2008). Moreover, climatology maps are a required element in searching for climate change signals, to evaluate climatic models and to understand how the climate interacts with other natural elements (Hofstra *et al.*, 2008). According to the World Meteorological Organization, climatology maps should be developed using databases with recordings covering over 30 years. On the other hand, many research projects have pointed out that the reliability of climate analysis results increases when a high-quality, high spatial density dataset is used (Madden *et al.*, 1993; Jones *et al.*, 1999; Hofstra *et al.*, 2008; Cowtan and Way, 2014).

Traditionally, climatology maps are produced from the spatial interpolation from the scant weather station series to obtain regularly distributed climatic information over a defined area. This is because of the necessity of organising the climatic information into continuous spatial fields of data to reduce the lack of information in some areas due to the irregular spatial distribution of the weather stations (Jones and Hulme, 1996; Dai *et al.*, 1997; New *et al.*, 2000). Until now, there has been no uniform consensus regarding what the most adequate interpolation method for climatic variables might be, and the best ones vary as a function of the area where they are applied and the interpolated variable (Vicente-Serrano *et al.*, 2003). On the other hand, various methods for evaluating their performance have been proposed during the last few decades (Kurtzman and Kadmon, 1999; Goovaerts, 2000; Vicente-Serrano *et al.*, 2003; Ninyerola *et al.*, 2007; Hofstra *et al.*, 2008; Li and Heap, 2011; Herrera *et al.*, 2012).

Generally speaking, interpolation methods can be subdivided into four main groups: global, local, geostatistical and hybrid (Vicente-Serrano *et al.*, 2003). Global methods (*e.g.* trend surface analysis and the regression models) use all the available spatial information to estimate the climatic values of the grid generated. These methods relate climate information with geographic data (elevation, latitude, slope, etc.) to generate the interpolated maps (Pons, 1996; Ninyerola *et al.*, 2000). On the contrary, local methods (such as Inverse

Distance Weighting, Nearest Neighbours, Delauny Thiessen and Minimum-curvature-splines) only make use of the information obtained from subsets from neighbouring stations; they usually assign weights to individual stations according to a function that combines distance from the point to be estimated and other characteristics or properties of neighbouring stations, such as the Angular Distance Weighted method and Correlation Decay Distance index (New *et al.*, 2000; Mitchell and Jones, 2005; Caesar *et al.*, 2006; Hofstra *et al.*, 2008).The geostatistical methods, like the Simple Kriging (Hengl *et al.*, 2004), Ordinary Kriging (Goovaerts, 2000), Co-Kriging (Nalder and Wein, 1998), Universal Kriging (Hosseini *et al.*, 1993) or Regression Kriging (Hengl, 2007; Hengl*et al.*, 2007), assume that the spatial variability of a continuous variable (or at least part of it) is too irregular to be modeled by a mathematical function, and could be better predicted by a probabilistic surface (Vicente-Serrano *et al.*, 2003). Lastly, hybrid methods combine elements from the above techniques to enhance the interpolation results (Ninyerola *et al.*, 2007).

In this paper, we developed a new high resolution climatology for monthly mean values of maximum (Tmax) and minimum (Tmin) temperature in the western Mediterranean basin (mainland Spain) by using a recent high quality, high density dataset (acronym MOTEDAS, Monthly Temperature Dataset of Spain; Gonzalez-Hidalgo *et al.*, 2015a). The new climatology emerges after comparing some of the best performing interpolation techniques, and the global results are shown in a complete collection of monthly maps of monthly mean maximum (Tmax), monthly mean minimum (Tmin) and monthly mean amplitude (Diurnal Temperature Range, DTR). The paper is organized as follows: in sections 2 and 3 we briefly describe the study area (Iberian Peninsula) and the dataset used in the new climatology; in section 4 we present the three interpolation methods and the error measurements used to estimate the performance of each one. Section 5 contains the accuracy of the models and their spatial differences by comparing various error measurements in several elevation bands, and concludes with the presentation of the new climatology and the collection of charts obtained from the best performing method. In section 6, we discuss the main findings and present the main conclusion.

2. **Study area**

The Spanish mainland (Iberian Peninsula, western Mediterranean basin) seems to be an appropriate area for evaluating the differences between interpolating approaches to temperature for several reasons. Firstly, its latitudinal position in the subtropical band suggests highly contrasting seasonal temperature regimes, while the north-south extension (c. 1000 km) introduces a reasonable gradient in the amounts of incoming solar radiation; on the other hand, the Iberian Peninsula has sharply contrasting landscapes, well-defined by altitude combined with orography: the coastland areas (<200 m above sea level, asl), the inland plateau (200-1000 m asl), and the high mountain areas (>1000 m asl); finally the Iberian Peninsula is located between two heavily contrasting water masses (Atlantic Ocean and Mediterranean Sea). As a consequence, large areas in the inland plateau regions (*meseta norte* and *meseta sur* in Spanish), are only open to Atlantic influences from the west, due to the alignment of the mountain systems, which are arranged in a west-east direction, bound on the eastern side by a north-south oriented chain, the Sistema Iberico (see Figure 1). These reasons, among others, result in a marked complexity in spatial distribution of temperature across the Iberian Peninsula, as indicated in classic publications (Font Tullot, 1983; Capel Molina, 1998; Sánchez and Sánchez, 1999). As a consequence, the local multivariate regression models can be expected to be much more suitable than global methods to estimate the spatial gradients of temperatures in the Spanish mainland, and also to provide easier interpretation of factors that contribute to spatial distribution of temperatures. Such local methods have been applied with optimal results in territories characterized by complex orography (Daly *et al.*, 2008; Frei, 2013; Brunetti *et al.*, 2014) but not yet, to our knowledge, in the Spanish mainland.

3. Data

We have developed the new climatology of temperatures following the global approach of Mitchell and Jones (2005) and using the most recently updated database of monthly temperatures, the MOTEDAS dataset (Gonzalez-Hidalgo *et al.* 2015a). MOTEDAS was developed after exhaustive analyses of the complete information stored at the National Meteorological Agency of Spain (AEMet). Quality control included detection of suspicious data and correction of inhomogeneities on a monthly scale (details in Gonzalez-Hidalgo et al. 2015a). The MOTEDAS high resolution grid (10 x 10 km) had previously been used to analyse the spatial variability of monthly temperatures and their trends at high resolution (Peña-Angulo *et al.*, 2015, Gonzalez-Hidalgo *et al.*, 2015b). In this research, we used the complete information included in the MOTEDAS dataset, in an attempt to maximize the information from the 3066 original series from AEMet, which contains at least 84 months of original data. These series were also checked by complementary quality control on their location (checks that were not included in the original development of MOTEDAS). In short, the locations of the 3066 stations were compared with a Digital Elevation Model (DEM) obtained from the ASTER-based Global Digital Elevation Model (GDEM) at a resolution of 30 m (Hayakawa *et al.*, 2008). These one-by-one-degree files can be downloaded from NASA's EOS data archive and/or Japan's Ground Data System (http://gdem.ersdac.jspacesystems.or.jp/). The stations were eventually discarded from the final data set for climatology reconstruction if the following three criteria were satisfied: (1) difference in altitude >150 m between official coordinates and DEM, (2) the altitude of the station did not correspond with any point of the DEM in the surrounding 2 km^2, and (3) the difference in the annual temperature mean value with respect to neighbouring stations was higher than 3ºC, taking into account the lapse rate by altitudes. In the end, a small percentage of the original series from MOTEDAS was discarded from the original 3066 stations (54 for Tmax and 45 for Tmin).

The final series (in terms of data availability) from MOTEDAS used in the development of temperature climatology were characterized as follows:

- Series with original complete information between 1951 and 2010 (11 stations).
- Series in which complete reconstruction was achieved between 1951-2010 with reference series from neighbouring stations no further away than 100 km (2865 stations in Tmax and 2869 in Tmin).
- Finally, in order to maximize the spatial information, the series in which MOTEDAS made an incomplete reconstruction but contained more than 7 years of original information between 1951-2010, were reconstructed following the approach suggested by (Brunetti *et al.* 2014). A total of 136 stations for Tmax and 141 of Tmin stations were saved using this procedure.

The final dataset includes 40% of original and 60% of reconstructed data from stations no further than 25 km apart. Obviously individual station data varies, depending on the area and decade, with original data showing an increase in the 1981-2010 period.

Consequently, the version of MOTEDAS used to develop the new temperature climatology of the Spanish mainland includes a total number of 3012 for Tmax and 3021 for Tmin of complete, homogeneous and free from suspicious data monthly series (1951-2010; see Figure 2), and offers a significantly higher station density than those used in several previous climatologies for the Spanish mainland (1068 stations used by Ninyerola *et al.*, 2005), and for the complete Iberian Peninsula (1440 stations used by Ninyerola *et al.*, 2007; 237 stations used by Herrera *et al.*, 2012). This procedure ensures that there is a reduced error bias in the series since a strong trend is displayed over the 1951-2010 period (see Gonzalez-Hidalgo et al., 2015a and b), and if station climate normals are calculated only from available data, the final result will be biased point by point, depending on the bias for the period covered by data from the stations surrounding each grid point.

4. Interpolation methods

Three different interpolation methods were compared: (1) Locally Weighted Linear Regression (LWLR), (2) Regression-Kriging (RK) and (3) Regression-Kriging with Stepwise selection (RKS). The resulting monthly Tmax and Tmin maps have a resolution of 0.0083º (~1 km at Iberian Peninsula latitude), which matches the spatial resolution of the GTOPO30 (USGS, 1996) Digital Elevation Model (DEM) on which the climatologies were reconstructed.

The DEM was used to assign geographic information to the stations, in addition to the elevation already available from station metadata together with latitude and longitude. For each cell of the DEM, we estimated the slope orientation, slope steepness and crossed distance from the sea (obtained by minimizing the sum of the cell-sea horizontal distance plus all vertical gradients crossed by the cell-sea segment) using the method described by (Brunetti *et al.*, 2014) and we assigned the geographical parameters of the closest grid cell to each station.

4.1. Local Weighted Linear Regression (LWLR)

The LWLR estimates locally the relationship between temperature and elevation (Brunetti *et al.*, 2014), which represents an improvement on the geographically weighted regression (GWR) approach (Brunsdon *et al.*, 1996) A weighted linear regression (Taylor, 1997), with neighbouring stations to predict the temperature (T) value of a cell (λ, ∅) as a function of the elevation, was estimated as follows:

$$T(\lambda,\emptyset) = a(\lambda,\emptyset) + b(\lambda,\emptyset) * h(\lambda,\emptyset) \qquad \text{(Eq. 1)}$$

where $a(\lambda,\emptyset)$ and $b(\lambda,\emptyset)$ are the linear regression coefficients, and $h(\lambda,\emptyset)$ the elevation.

The basic idea of the approach is to evaluate the relationship between temperature and elevation separately for each grid cell of the DEM, giving more importance to any nearby stations with topographical characteristics similar to those of the grid cell itself. Specifically, a number of neighbouring stations (at least 15 and no more than 35, - 35 being the number that minimizes the error) with the highest weights were used in the estimation of the regression for each grid point *$(\lambda,\emptyset)$*. The minimum and maximum number of neighbouring stations considered was determined by an analysis of interpolation accuracy by Root Mean Squared Error (RMSE). For each station, the weight was calculated as the product of the following weighting factors:

$$w_i(\lambda,\emptyset) = w_i^r(\lambda,\emptyset) * w_i^h(\lambda,\emptyset) * w_i^{dsea}(\lambda,\emptyset) * w_i^{slope}(\lambda,\emptyset) * w_i^{aspect}(\lambda,\emptyset) \qquad \textit{(Eq. 2)}$$

These weighting factors (position, height, distance from the sea, slope steepness and slope orientation) are based on Gaussian functions of the form:

$$\mathrm{w_i^{var}}(\lambda,\emptyset) = \mathrm{e}^{-\left(\frac{\Delta_i^{var}(\lambda,\emptyset)^2}{c_{var}}\right)} \qquad \text{(Eq. 3)}$$

where Δ_i^{var} is the absolute value of the difference between the value of the specific variable in cell $(\lambda,\emptyset)$ and in the i-th station, and c_{var} is a coefficient that expresses the decrease of the weighting function with increasing Δ_i^{var}. The c_{var} coefficients can also be expressed in terms of the value $\Delta_{\frac{1}{2}}^{var}$ which represent the value of Δ_i^{var} for which the weighting factor is equal to 0.5.

$$c_{var} = -\frac{(\Delta_{\frac{1}{2}}^{var})^2}{\ln 2} \qquad \text{(Eq. 4)}$$

To select the most appropriate $\Delta_{\frac{1}{2}}^{var}$ values to be used in the weighting factors, we followed an iterative process, and the $\Delta_{\frac{1}{2}}^{var}$ producing the lowest possible error at station locations was estimated for each month.

The most relevant weight is the radial, which is the optimization of the $\Delta_{\frac{1}{2}}^{r}$ factor producing the largest improvement in interpolation performance. Its optimal values vary from month to month, with lower values in summer (24 km in July) and higher in winter (58 km in February) for Tmax; on the contrary, for Tmin, lower values were found in winter (18 km from November to February), and higher values in spring and summer (24 km from April to July).

The other halving factors ($\Delta_{1/2}^{h}$, $\Delta_{1/2}^{dsea}$, $\Delta_{1/2}^{slope}$, $\Delta_{1/2}^{aspect}$) were set as in Brunetti *et al.*(2014).

4.2. Regression-Kriging (RK)

The RK method combines a regression model with a Kriging (Hengl *et al.* 2007) of the regression residuals (Tveito *et al.*, 2008; Di Piazza *et al.,* 2011; Brunetti *et al.*, 2014).

In this case, we first estimated the temperature vs. elevation (*h*) linear regression model as in Eq. 1, but with a global approach, i.e. with *a* and *b* coefficients identical for each grid cell and dependent only on the month in question. A Kriging interpolation was then applied to the residuals from this model. This technique can be used to obtain a variogram providing information on the spatial correlation of the analysed residuals. In this study, we took into account all pairs of stations in the range of 250 km, and grouped them according to distance intervals of 10 Km. The exponential variogram was selected to model the dependency between the semivariance and the distance, as this provided the lowest error.

The theoretical variogram was used to obtain the covariance (C) vs distance, and the covariance matrix, expressing the covariance of any pair of stations. The array with the Kriging weights ($\boldsymbol{k}$) for each cell $(\lambda, \emptyset)$ was obtained as follows:

$$\boldsymbol{k}(\lambda, \emptyset) = \boldsymbol{C}^{-1} * \boldsymbol{c_0}(\lambda, \emptyset) \qquad \text{(Eq. 5)}$$

where $\boldsymbol{c_0}$ is the array representing the covariance of the cell $(\lambda, \emptyset)$ with all the station positions. The temperature of each cell was thus estimated as follows:

$$T = a + b * \mathrm{h}(\lambda, \emptyset) + \boldsymbol{k}^{\boldsymbol{T}}(\lambda, \emptyset) * \boldsymbol{\epsilon} \qquad \text{(Eq. 6)}$$

where a and b are parameters defined by the global regression model, h is the elevation, $\boldsymbol{k}^{\boldsymbol{T}}$ is the vector of the Kriging weights, and $\boldsymbol{\epsilon}$ the vector of station residuals.

4.3. Regression Kriging with Stepwise selection (RKS)

The third interpolation method used in this study was a variation of the previously described RK. In this case the Kriging is used to interpolate the residuals from a multi-linear regression model (slope steepness, slope orientation, distance from the sea, altitude, longitude, and latitude) with stepwise selection. The stepwise selection method allows us to choose the optimum independent variables that will be used in the multi-linear regression model for each month. This method integrates the variables in an iterative way: in each step it evaluates which set of variables should be included in the model. The algorithm stops when the model does not make any further improvements, either by introducing or removing variables. The relative quality of the model is evaluated with Akaike's information criterion (AIC). The AIC is a measure of the relative quality of a fitting model. The lower the AIC value, the better the model.

As in the previous method, a Kriging interpolation was applied to the residuals from the multi-linear regression. To this end, all pairs of stations in the range of 250 km were taken and grouped according to distance intervals of 10 km. Finally, we selected the exponential variogram to model the dependency between the semivariance and the distance.

In this way, the temperature in each cell was estimated by the following equation:

$$T = a + b * h(\lambda, \emptyset) + c * \lambda + d * \emptyset + e * slope(\lambda, \emptyset) + f * aspect(\lambda, \emptyset) + g * dsea(\lambda, \emptyset) + \\ + \boldsymbol{k}^{\boldsymbol{T}}(\lambda, \emptyset) * \boldsymbol{\epsilon}$$

(Eq. 7)

where coefficients a, b …, g not excluded by the stepwise selection iterative procedure were determined with the regression model.

4.4. Validation procedure and error measurements

The performances of the three interpolation models were evaluated by using a leave-one-out validation procedure; the monthly value from each station was excluded from the dataset and reconstructed by the three models, using all the other stations; finally, the estimated value was compared with the observed value. This procedure ensured a higher level of accuracy with respect to the classic approach of leaving a fixed percentage of original data for the validation procedure, because in the leave-one-out, all the original data involved in the model are checked individually with their specific model.

Four error measures were computed to compare the performances of the interpolation methods: the Mean Bias Error (MBE), the Mean Absolute Error (MAE), the Root Mean Squared Error (RMSE), and the Index of Agreement (D) developed by (Willmott 1982).The MBE provides information on the tendency of the model to systematically overestimate or underestimate a variable (Pielke, 1984). The Mean Absolute Error (MAE) is the average of the differences (in terms of absolute value) between that observed and that predicted by the model. The Root Mean Squared Error (RMSE) estimates the average difference between estimated and observed values in each station. The RMSE and MAE summarize the average difference between the estimated and real values with the same units (Vicente-Serrano *et al.*, 2003); Willmott (1982) suggested that RMSE was more appropriate than MAE in order to validate spatial interpolation models, although Vicente-Serrano *et al.* (2003) indicated that MAE is less sensitive than RMSE when dealing with extreme values. In this respect, RMSE is stricter than MAE. The Index of Agreement (D) is a standardized measure of the model prediction error and varies between 0 and 1. A value of 1 indicates a perfect match, and 0 indicates no agreement at all (Willmott, 1982). Index D can detect proportional differences in the observed and estimated means and variances; however, it is too sensitive to extreme values, due to the squared differences (Legates and McCabe, 1999).

Finally, the global quality of the model was also evaluated by the coefficient of determination (R^2) as a square of the multiple Pearson correlation coefficient. This coefficient not only gives information on the quality of a model, but also on its capacity for prediction under the assumption of explained variance.

5. Results

5.1. Global accuracy of models

The global results of interpolation methods evaluated by various error measurements (MBE, MAE, RMSE, R^2 and D) are shown in Tables 1 and 2 for Tmax and Tmin on an annual and monthly scale. The performances are better for Tmax than for Tmin, both on a monthly and annual scale, with MAE and RMSE being lower for Tmax than for Tmin, and the reverse being true for D and R^2 (Tables 1 and 2).

Errors are always maximum in summer, for both Tmax and Tmin, and the lowest errors are in winter for Tmax and in spring for Tmin. In particular, the highest values of RSME range from 1.16 to 1.27°C in July for Tmax, and from 1.26 to 1.32°C in August for Tmin, while its lowest values range from 0.81 to 0.83°C in February for Tmax and from 0.97 to 1.05°C in April for Tmin. The lowest RMSE values of these ranges are those from the LWLR method. The same annual cycle in RMSE, but with higher values, was presented in the previous climatology of the Spanish mainland by (Ninyerola *et al.*, 2005), in which the lowest RMSE values were 1.6°C in July for Tmax and 1.5°C in August for Tmin, and its highest values were 1.1°C in February for Tmax and 1.1 in April for Tmin. These results can also be deduced from the MAE, R^2 and D. These findings coincide with the spatial variability of temperatures evaluated by the Correlation Distance Decay by (Peña-Angulo *et al.*, 2015), with the lowest

RMSE values relating to the months characterized by highest spatial coherence.

In the Spanish mainland, the best performing model is always the LWLR, and the worst is the RK. Differences among models are much more evident for Tmin than for Tmax. Looking at RMSE, there is a maximum range between best and worst performing method of about 0.1°C in summer for Tmax and about 0.2°C in autumn for Tmin. The MAE (ºC) also shows that the lowest error is returned by the LWLR method, where values between 0.61 and 0.88 are achieved according to the month; in second place is the RKS, with values between 0.60 and 0.89; and finally the RK between 0.61 and 0.94.

5.2. Performance of the models vs elevation

These global results must be taken with caution, since they refer to a very complex terrain in which the effects of distance from water bodies, altitude, and latitude are combined. In particular, we verified whether the accuracy of the models for Tmax and Tmin changes with altitude. Figure 3 shows the mean annual values of MBE for different elevation bands, together with January and July. This estimator allows us to identify systematic over/under estimations. In general, the three models produce lower MBE at low altitude, but MBE values increase in the highlands, particularly above 1000 m asl, where there is a systematic overestimation of Tmax, and a systematic underestimation of Tmin. This phenomenon is important for RK and RKS, where bias can reach several tenths of a degree for the highest elevation bands (with Tmax/Tmin biases of +0.58/-0.93°C and +0.49/-0.63°C above 1200m for RK and RKS respectively), but much lower for the LWLR method (Figure 3). The same pattern was observed in the other error measurements (figure not shown).

The analyses of monthly model performance versus altitude show differences between cold and warm months and the systematic errors in the various elevation bands are much more evident. In Figure 3, the January and July (as representative of cold and warm periods) monthly values of MBE for LWLR, RK and RKS at different altitude intervals are shown, which roughly correspond to coastland areas (<200 m asl), inland plateaus and inland catchments (200-1000 m asl), and mountain landscapes (>1000 m asl).

The negative systematic biases at high elevation bands for Tmin range between -0.61°C and -1.20°C in the RK model, in summer and winter respectively. On the contrary, LWLR presents lower biases in winter than in summer, with values ranging from -0.11°C in winter to -0.19°C in summer. RKS has minimum biases in spring (-0.43°C) and maximum in autumn (-0.83°C). As for Tmax , monthly biases above 1200 m asl are negative in winter and positive from March to November (not shown in the figure) for RK (ranging from -0.33°C in December to +1.28°C in July), and always positive for RKS (ranging from +0.08°C in December to +0.73 in July). No relevant biases are observed for Tmax in the LWLR model.

In low elevation bands, systematic errors are smaller or absent, depending on the model and the season. LWLR presents no systematic errors below 1000 m in any month, either for Tmax or Tmin, and biases are always lower than 0.1°C (negative or positive). RK, on the contrary, has positive (negative) systematic biases, up to +0.2°C (-0.2°C) in winter (summer) months for Tmin (Tmax). The same is true for RKS, with errors up to +0.17°C in autumn Tmin and up to -0.15 in summer Tmin.

5.3. Climatology maps of maximum and minimum temperature, and DTR.

The classic analyses of spatial distribution of Tmax and Tmin in the Spanish mainland (Font Tullot, 1983, Capel Molina, 1998), and the most recent climatologies (Ninyerola *et al.*, 2007, AEMet, 2011), have shown that the spatial distribution of the isotherms in the Iberian Peninsula varies according to the latitude, distance from the sea and elevation, with large spatial variations throughout the year, i.e.: temperatures increase from north to south, in coastal areas the gradients are smoothed, and the orography is the principal factor driving the spatial distribution of Tmax and Tmin values. Furthermore, due to the west-east orientation of the mountain systems and the fact that the inland plateaus are open to the west (see Figure 1), the influence of the Atlantic Ocean on temperatures spreads over a large area of inland Spain to the east, while the influence of the Mediterranean is limited to a small area, due to the vicinity of the mountain systems in the southern and eastern coastal areas; this leads to a second main gradient from west to east being identified in the classic maps.

The above results suggest that the global method (such as RK and RKS) are not the most suitable for capturing the complex interrelation of these factors affecting the temperature spatial gradients in the Spanish mainland and causing the near-surface temperature to change significantly from region to region. Our results indicate that the most adequate approach is a local estimate of the temperature lapse rate, made by using the information from the most representative stations in that location, as the LWLR method does. In the following paragraphs, we will take the climatologies produced with the LWLR approach as the base of reference for the Spanish mainland, and describe their main features.

5.3.1. The Tmax climatology

Tmax climatology maps are shown in figure 4 (see also Figure 1 for spatial identification).

During winter (December to February), most of the Spanish mainland has Tmax values below 15ºC, except for small areas in the extreme coastland to the south-west and east. The inland Tmax spatial distribution is characterized by the contrast between inland catchments and their mountain borders with the Mediterranean and south-west coastland areas, with the isotherm of 15ºC as a limit. The Tmax mean value in the northern plateau (Duero basin) is lower (<10ºC) than in the southern inland catchments of Tagus, Guadiana and Guadalquivir, and the Ebro inland in the north-east (>10ºC). Finally, in the southern plateau (but not in the northern inland Duero catchment) a clear west-east gradient is identified, accentuated during the month of February. Month by month, the areas below 10ºC are restricted to the mountain regions and eastern part of the northern Duero basin.

Between March and May, the north-south gradient remains between inland catchments; in southern ones, Tmax values above 20ºC are found in March in the southernmost areas (Guadalquivir basin) and extend to the rest of the southern catchment and Ebro basin to the north-east during April and May; the Duero catchment, in the northern plateau, reaches an isothermal value of 20ºC only in May in its western area, one month later than the other inland areas. The Tmax value in the north-eastern Ebro basin is quite similar to the southern catchment, i.e. the latitude (quite similar to the Duero basin) does not seem to be a determining factor for Tmax during these months. In April and May, Tmax values below 15ºC are found only in mountain areas and the eastern Duero catchment in the northern inland plateau. The coastland areas behave in a different way, depending on their position (Atlantic versus Mediterranean water bodies). In the Mediterranean coastland to the east and in the south, Tmax is above 20ºC, while in the northern coastland it is >15ºC. Month by month, Tmax values above 25ºC increase along the axis of the main rivers (Tagus, Guadiana, Guadalquivir and Segura catchment). In May, the value of Tmax in the Spanish mainland is above 20ºC, except in mountain areas and the northern coast.

The warm season lasts from June to September, and a clear north-south gradient is detected in Tmax, with mountain areas isolated from the surrounding landscapes by the isothermal value of 20ºC. The maximum values of Tmax are found in the southern plateau and central area of the Ebro basin to the north-east (>30ºC). The coastal areas differ again between Atlantic and Mediterranean, with the Mediterranean coastland presenting Tmax values similar to inland southern catchments.

June and September show a similar spatial distribution of Tmax values. In both cases, the north-south separation is defined by the 25ºC isotherm and, in extended areas of the southern Spanish mainland, Tmax is above 25ºC. On the other hand, the spatial distribution of Tmax in July and August is quite similar, showing the same north-south gradient, with the threshold between north and south being the 30ºC isotherm. In the southern inland areas, Tmax values are >35ºC.

October and November seem to be transitional months. During October the Tmax spatial distribution resembles that of the warmest months (north-south gradient, differences between coastal areas, isolated mountain areas) with lower mean values. The coastland-inland and north-south gradients are clearly separated by the 20ºC isotherm in October, and 15ºC in November. In the highland inland areas, Tmax values are below 15ºC. Globally, the spatial distribution of Tmax in October is similar to May, and November to March. Finally, in November the inland northern Duero basin Tmax is similar to the surrounding mountain areas where, in the highest places, it falls below 5ºC.

Only in the Mediterranean coastal and south-western areas are Tmax values above 15ºC.

In brief, Tmax spatial monthly distribution shows a north-south gradient in the inland catchments, accentuated during the warmest months by a higher increase in southern Tmax values. Mountain areas in the warmest months are cold and isolated from the surrounding areas, i.e. altitude affects spatial variability of Tmax, particularly when solar radiation is at maximum. In addition to a north to south gradient, there is also a west-east gradient. This combination of latitudinal gradient and relative position (oriented to sea influences from the west or east) seems to explain the differences between catchments located at the same latitude, such as the Duero and Ebro: a combination of the sheltering effect of mountain systems, prevalent westerly wind circulation and different effects from the Atlantic and Mediterranean water bodies emerge as a plausible explanation of Tmax differences between the Duero and Ebro basins located at the same latitude.

5.3.2. Tmin climatology

Tmin climatology maps are shown in figure 5 (see also Figure 1 for spatial identification).

In general, the spatial differences of Tmin values are lower than for Tmax and this is particularly true during the warmest months producing a monthly amplitude (Tmax-Tmin) spatially variable throughout the year (see below).

From November to April, the spatial distribution of Tmin is similar and most of the Spanish conterminous land is below 5ºC, except in small areas in the eastern and southern coastland. The lowest values can be found in December, January and February in mountain areas and the Duero basin in the northern plateau (Tmin below 0ºC), with a clear north to south gradient, while the southern inland catchments and Ebro basin to the north-east are above 0ºC. In the southern catchments of the Tagus, Guadiana and Guadalquivir, a west-east gradient in Tmin is detected. The differences between coastal and inland areas are lower than for Tmax. In November, March and April the area between 5ºC and 10ºC in Tmin extends to the south-west. The <0ºC value of Tmin is restricted to mountain areas in March and April.

In May, the spatial distribution of Tmin along the north–south gradient between catchments (10ºC as a limit between north and south) is more complex; the Ebro basin exhibits similar values to southern basins (>10ºC) and in the southern part of the Spanish mainland there is a west to east gradient. During May, the 10ºC isotherm moves inland from the SW of the southern catchments and Mediterranean coastal areas, while northern coastland Tmin values are <10ºC.

The warmest period from June to September shows a clear north-south gradient with the 15ºC isotherm separating the north from the south in July-August, and 10ºC in June and September. Tmin values of <5ºC are restricted to mountain areas and the 15ºC isotherm also seems to be the boundary between inland and coastal to the east and south. Except for July and August, Tmin values in the Ebro basin are similar to the Duero basin at the same latitude.

In brief, the spatial differences of Tmin values seem lower than Tmax. In addition, north-to-south, west-to-east or east-to-west gradients according to latitudinal position and proximity of different water bodies, are simplified.

5.3.3. The DTR climatology

Lastly, Figure 6 shows the DTR monthly collection charts. Generally speaking, during the warmest months (June to September) there is a clear inland-coastland gradient in the DTR values, which are higher inland. Along the Mediterranean fringe and northern coastland the DTR values vary between 6ºC-8ºC, while inland they vary between 10ºC -12ºC, (see Figure 6), with maximum values over 18ºC.

The coastland-inland pattern during October-February disappears, when the lowest DTR values of 6ºC to 8ºC are found in the northern coastal areas, and increase toward the central inland and southern areas, where the monthly DTR is 10ºC to 12ºC. From March to May, the Atlantic coastland to the north and west differs from the Mediterranean southern coastland, with DTR values lower in the Atlantic coastal area (6ºC - 8ºC) than the Mediterranean eastern coast (10ºC - 12ºC). The inland areas show DTR between 6ºC and 12ºC. In May, the DTR values inland are over 14ºC.

In brief, the DTR monthly spatial distribution indicates that the maximum values are reached inland during the summer months when there is a clear difference between coastal and inland areas. During the coldest months this pattern disappears, and a north-south gradient predominates in the DTR monthly values, increasing toward the south. The maximum spatial differences in DTR values have been found in July and August (coastland 6ºC-8ºC, inland >18ºC); meanwhile during the coldest months, the maximum spatial differences vary between 4ºC-6ºC in coastal areas and 8ºC-10ºC inland. A plausible explanation is that Tmax in the coldest months is strongly affected by factors such as air humidity or cloud to a higher degree than those factors that can promote spatial variability in Tmin.

6. Discussion and conclusions

6.1. Global comments

We applied different interpolation approaches to the recent high quality and up-to-date monthly temperatures dataset of Spain (MOTEDAS), with the aim of producing a new high resolution climatology for Tmax and Tmin in the Spanish mainland. The poorest results were observed in summer for both Tmax and Tmin data, while better results were found in winter for Tmax and in spring for Tmin. The comparison between models indicates that the estimation errors vary as a function of the altitude and a generalized underestimation/overestimation of Tmin/Tmax was detected particularly at >1000 m where the LWLR method performed best.

The quality of dataset used and the high spatial density of stations in this research is probably the most relevant reason for the general improvement of the RMSE with respect to previous climatologies (Ninyerola *et al.*, 2005), or when comparing the R^2 coefficients of annual mean values obtained from 1350 stations (Ninyerola *et al.* 2007), with those obtained in this research (see Tables 1 and 2). Therefore, all the three methods applied are an improvement on previous results.

The global difference between the performance of the models for Tmax and Tmin can be attributed to the various factors affecting these, because Tmax depends more on global factors, such as radiation defined by latitudinal position, while Tmin could be more heavily affected by local factors, such as land use associated with the albedo, latent heat fluxes etc. (Christy *et al.*, 2009; Klotzbach *et al.*, 2009; McNider *et al.*, 2010), which are more difficult to implement in the models and not always captured by the available station data. Within this context it would be interesting to verify whether the three methods produce systematic errors at a local level, when selected station clusters are included.

All three models produced the worst results in highland areas, particularly for Tmin in summer. Again, the LWLR returned the best results, in particular above 1000 m asl for both Tmax and Tmin (Figure 3). The worst model is RK and it is interesting to note the improvements provided by the introduction of the stepwise selection method in the RKS model, which means that the introduction of additional variables to estimate temperature fields in the different months gives better results, in Tmax during summer and in Tmin, in particular, during winter. The relevance of the variables differs from month to month, also between Tmax and Tmin. The slope orientation was considered only for Tmax in the cold months (January, December, and in October) and September. In February, the distance from the sea was not included in the model, while in November the longitude was excluded. With Tmin, all the geographic variables were relevant in the model except for the longitude in April.

The analyses of the coefficients of the multilinear regression allowed us to compare the role of the different independent variables (predictors) on Tmax and Tmin. The elevation effect (representing the global lapse rate) is stronger in spring and autumn for Tmax and in summer for Tmin. The latitude coefficients show a higher effect on temperature in summer (both for Tmax and Tmin) and more for Tmax than Tmin, according to a strict relationship with incoming solar radiation. The effect of slope steepness is positive in Tmin in all months, and negative in Tmax between March-October. In Tmax, the maximum effect of slope was found during summer, while in Tmin the strongest effect was found in cold months. Slope orientation is positive in all months and more important in winter in Tmin, while it seems to be less relevant for Tmax; also distance from the sea is more significant during summer than winter.

The overall spatial variability of temperatures and the relevance of different geographical variables, in addition to the elevation, in driving this variability has been well identified by several models for the Spanish mainland. Ninyerola et al. (2005, 2007) applied a combination of a multiple regression with residuals correction by means of local and geostatistical techniques, while the

Spanish Meteorological Agency (AEMet, 2011) applied a multivariate regression interpolation method with a residuals correction, performed with either a local (Inverse Distance Weighted) or a geostatistical method (Simple Kriging).

However, as well as the different role of these variables throughout the year, there is an important spatial variability in their effect on temperature. This is demonstrated by the fact that the local approach of the LWLR model (which includes all the variables in the station weighting procedure) allows for the spatial variability of the temperature lapse rate (linked to the geographical aspects) to be better captured in the different months of the year, providing lower errors at each elevation band, even without any further interpolation of the residuals.

6.2. Final remarks

The new approach proposed in the present paper by using LWLR seems to be an improvement on the previous ones, at the present level of development of interpolation techniques, due to the decrease in the global error values (at high altitude in particular) and, even more important, because of the elimination of systematic biases at different elevation bands.

In conclusion, the analyses of error measurements and their spatial and temporal distribution indicated that the approach proposed in this paper, the LWLR method, as compared to the generalized RK and the RKS, improves the previous climatologies in the Spanish mainland, and should be suggested for future research.

Nevertheless, even though in our case LWLR turned out to be the most appropriate approach, this result cannot be generalized. In particular, the LWLR method is more dependent on the availability of station data than RK and RKS and any global approach in general. For other datasets, RK and RKS may be more suitable, either because they are simpler to use or because station density is not sufficient to apply LWLR.

As well as better performance in terms of station errors, LWLR has the additional advantage of estimating a prediction interval for any grid point in the terrain studied. Since LWLR uses weighted linear regression to estimate temperature as a function of elevation, standard methods for calculating prediction intervals for the dependent variable can be used as in Daly *et* *al.*(2008). The procedure consists in estimating the variance of the temperature (T) of a grid-point at elevation *h* as:

$$s^2\{T_h\} = s^2\{\hat{T}_h\} + MSE \qquad (8)$$

where MSE is the mean square error of the observed station temperatures compared to those obtained with the regression model.

This estimation takes into account both the variation in the possible location of the expected temperature for a given elevation ($s^2\{\hat{T}_h\}$) linked to the regression coefficient errors and the variation of the individual station temperatures around the regression line (MSE).

Expressing $s^2\{\hat{T}_h\}$ in terms of MSE, station weights (w_i, as defined in eq. 2) and station elevations (h_i), the following is obtained:

$$s^2\{T_h\} = MSE \cdot \left\{1 + \frac{1}{\Sigma w_i} + \frac{(h-\bar{h})^2}{\Sigma(w_i h_i - \bar{h})^2}\right\} \qquad (9)$$

where *i* ranges over the stations involved in the grid point reconstruction.

The prediction interval at significance level α can be estimated as:

$$T_h \pm t_{\frac{1-\alpha}{2},df} \cdot s\{T_h\} \qquad (10)$$

where *t* is the value of a Student distribution with *df* degrees of freedom corresponding to cumulative probability (1-α)/2.

In Figure 7, the 68% confidence interval (we chose 68% in order to find prediction intervals easily comparable with the station leave-one-out RMSE) for January and July is presented as an example. The confidence interval is higher in summer than in winter and for Tmin than for Tmax, i.e. when the spatial coherence is lower. These maps allow us to understand where station density should be enhanced to improve confidence in the reconstruction.

The most critical areas are mountains in summer for Tmax, while Tmin seems to be more sensitive to station density, showing higher confidence intervals where station density is lower.

These are the areas where the new climatology should be taken with more caution, not only because of the scarcity of stations to validate any model, but also as a consequence of the larger confidence interval of the model algorithms in these areas.

We offer a collection of monthly charts for the Spanish mainland for the period between 1951 and 2010. The climatology is available upon request.

Acknowledgments

This study was supported by the Ministry of Science and Innovation, (Spanish Government), projects: the Hydrological Impacts of Global Warming in Spain (HIDROCAES, CGL2011-27574-C02-01) and the Development of Drought Index in Spain (DESEMON, CGL2014-52135-C3-3-R); Gobierno Regional de Aragón DGA-FSE (Grupo de Investigación Consolidado "Clima, Agua, Cambio Global y Sistemas Naturales"). Original data from AEMet (Spanish National Meteorological Agency).

References

AEMet, 2011. *Atlas climático ibérico/ Iberian climate atlas*. Agencia Estatal de Meteorología, Ministerio de Medio Ambiente y Medio Rural y Marino.Madrid.

Brunetti, M., Maugeri, M., Nanni, T., Simolo, C. and Spinoni, J., 2014. High-resolution temperature climatology for Italy: interpolation method intercomparison. *International Journal of Climatology*, 34 (4), 1278–1296.

Brunsdon C, Fotheringham AS, Charlton ME. 1996. Geographicallyweighted regression: a method for exploring spatial nonstationarity.*Geographical Analysis*, 28(4), 281–298.

Caesar, J., Alexander, L., and Vose, R., 2006. Large-scale changes in observe daily maximum and minimum temperatures: Creation and analysis of a new gridded data set. *Journal of Geophysical Research: Atmospheres*, 111 D05101. doi: 10.1029/2005jd006280.

Capel Molina, J.J., 1998. Ritmo anual de las temperaturas en España. *Nimbus*, 1-2, 17-36.

Christy, J.R., Norris, W.B. and McNider, R.T., 2009. Surface temperature variations in east Africa and possible causes. *Journal of Climate*, 22 (12), 3342–3356.

Cowtan, K. and Way, R.G., 2014. Coverage bias in the HadCRUT4 temperature series and its impact on recent temperature trends. *Quarterly Journal of the Royal Meteorological Society*, 140 (683), 1935–1944.

Dai, A., Fung, I.Y., and Del Genio, A.D., 1997. Surface observed global land precipitation variations during 1900-88. *Journal of Climate*, 10 (11), 2943–2962.

Daly, C., Halbleib, M., Smith, J.I., Gibson, W.P., Matthew K. Doggett, a G.H.T., Curtisb, J., and Pasteris, P.P., 2008. Physiographically sensitive mapping of climatological temperature and precipitation across the conterminous United States. *International Journal of Climatology*, 28, 2031–2064.

Di Piazza, A., Conti, F. Lo, Noto, L. V., Viola, F. and La Loggia, G., 2011. Comparative analysis of different techniques for spatial interpolation of rainfall data to create a serially complete monthly time series of precipitation for Sicily, Italy. *International Journal of Applied Earth Observation and Geoinformation*, 13 (3), 396–408.

Font Tullot, I., 1983. *Climatología de España y Portugal*. Ediciones Universidad de Salamanca, Salamanca.

Frei, C., 2013. Interpolation of temperature in a mountainous region using nonlinear profiles and non-Euclidean distances. *International Journal of Climatology*, 34 (5), 1585-1605. DOI: 10.1002/joc.3786.

Gonzalez-Hidalgo, J.C., Peña-Angulo, D., Brunetti, M. and Cortesi, N., 2015a. MOTEDAS: a new monthly temperature database for mainland Spain and the trend in temperature (1951-2010). *International Journal of Climatology*, DOI: 10.1002/joc.4298.

Gonzalez-Hidalgo, J.C., Peña-Angulo, D., Brunetti, M. and Cortesi, N., 2015b. Recent trend in temperature evolution in Spanish mainland (1951–2010): from warming to hiatus. *International Journal of Climatology*, DOI: 10.1002/joc.4519.

Goovaerts, P., 2000. Geostatistical approaches for incorporating elevation into the spatial interpolation of rainfall. *Journal of Hydrology*, 228 (1-2), 113–129.

Hayakawa, Y.S., Oguchi, T., and Lin, Z., 2008. Comparison of new and existing global digital elevation models: ASTER G-DEM and SRTM-3. *Geophysical Research Letters*, 35 L17404. Doi: 10.1029/2008gl035036.

Hengl, T., 2007. *A Practical Guide to Geostatistical Mapping of Environmental Variables.*JCR Scienctific and Technical Reports. European Community, Luxembourg. Available at http://spatial-analyst.net/book/, (ISBN 978-90-9024981-0).

Hengl, T., Heuvelink, G.B.M. and Rossiter, D.G., 2007. About regression-kriging: From equations to case studies. *Computers and Geosciences*, 33 (10), 1301–1315.

Hengl, T., Heuvelink, G.B.M. and Stein, A., 2004. A generic framework for spatial prediction of soil variables based on regression-kriging. *Geoderma*, 120 (1-2), 75–93.

Herrera, S., Gutiérrez, J.M., Ancell, R., Pons, M.R., Frías, M.D. and Fernández, J., 2012. Development and analysis of a 50-year high-resolution daily gridded precipitation dataset over Spain (Spain02). *International Journal of Climatology*, 32 (1), 74–85.

Hofstra, N., Haylock, M., New, M., Jones, P.,and Frei, C., 2008. Comparison of six methods for the interpolation of daily, European climate data. *Journal of Geophysical Research: Atmospheres*, 113 (21), D21110. Doi: 10.1029/2008jd010100.

Hosseini, E., Gallichand, J. and Caron, J., 1993. Comparison of several interpolators for smoothing hydraulic conductivity data in South West Iran. *American Society of Agricultural Engineers*, 36 (6), 1687–1693.

Jones, P.D. and Hulme, M., 1996. Calculating regional climatic time series for temperature and precipitation: Methods and illustrations. *International Journal of Climatology*, 16, 361–377.

Jones, P.D., New, M., Parker, D.E., Martin, S. and Rigor, I.G., 1999. Surface air temperature and its changes over the past 150 years. *Reviews of Geophysics*, 37 (2), 173–199.

Klotzbach, P.J., Pielke, R. a., Pielke, R.A., Christy, J.R. and McNider, R.T., 2009. An alternative explanation for differential temperature trends at the surface and in the lower troposphere. *Journal of Geophysical Research*, 114, D21102, doi:10.1029/2009JD011841.

Kurtzman, D. and Kadmon, R., 1999. Mapping of temperature variables in Israel: A comparison of different interpolation methods. *Climate Research*, 13 (1), 33–43.

Legates, D.R. and McCabe Jr., G.J., 1999. Evaluating the use of ‘goodness-of-fit’ measures in hydrologic and hydroclimatic model validation. *Water resources research*, 35 (1), 233–241.

Li, J. and Heap, A.D., 2011. A review of comparative studies of spatial interpolation methods in environmental sciences: Performance and impact factors. *Ecological Informatics*, 6 (3-4), 228–241.

Madden, R.A., Shea, D.J., Branstator, G.W., Tribbia, J.J., and Weber, R.O., 1993. The Effects of Imperfect Spatial and Temporal Sampling on Estimates of the Global Mean Temperature: Experiments with Model Data. *Jurnal of Climate*, 6, 1057–1066.

McNider, R.T., Christy, J.R., and Biazar, A, 2010. A stable boundary layer perspective on global temperature trends. *InIOP Conference Series: Earth and Environmental Science*, 13, 012003. Doi: 10.1008/1755-1315/13/1/012003.

Mitchell, T.D. and Jones, P.D., 2005. An improved method of constructing a database of monthly climate observations and associated high-resolution grids. *International Journal of Climatology*, 25 (6), 693–712.

Nalder, I.A. and Wein, R.W., 1998. Spatial interpolation of climatic Normals: test of a new method in the Canadian boreal forest. *Agricultural and Forest Meteorology*, 92, 211–225.

New, M., Hulme, M. and Jones, P., 2000. Representing twentieth-century space-time climate variability. Part II: Development of 1901-96 monthly grids of terrestrial surface climate. *Journal of Climate*, 13 (13), 2217–2238.

Ninyerola, M., Pons, X. and Roure, J.M., 2000. A Methodological Approach of Climatological Modelling of Air Temperature and Precipitation. *International Journal of Climatology*, 1841 (20), 1823–1841.

Ninyerola, M., Pons, X, and Roure, J.M., 2005. *Atlas climático digital de la Península Ibérica Metodología y aplicaciones en bioclimatología y geobotánica Información*. Universitat Autònoma de Barcelona Departament de Biologia Animal, Biologia Vegetal i Ecologia (Unitat de Botànica) Departament de Geografia. Barcelona, España.

Ninyerola, M., Pons, X. and Roure, J.M., 2007. Objective air temperature mapping for the Iberian Peninsula using spatial interpolation and GIS. *International Journal of Climatology*, 27, 1231–1242.

Peña-Angulo, D., Cortesi, N., Brunetti, M.and González-Hidalgo, J.C., 2015. Spatial variability of maximum and minimum monthly temperature in Spain during 1981–2010 evaluated by correlation decay distance (CDD). *Theorical and Applied Climatology*, 122, 35-45.

Pielke, R.A., 1984. Mesoscale Meteorological Modeling. *Quaterly Journal of the Royal Meteorological Society,* 111, 671-672.

Pons, X., 1996. Estimación de la Radiación Solar a partir de modelos digitales de elevaciones. Propuesta metodológica. *In*J. Juaristiand I Moro, eds. *VII Coloquio de Geografía Cuantitativa, Sistemas de Información Geográfica y Teledetección.* Vitoria-Gasteiz, Asociación de Geógrafis Españoles, 87–94.

Sánchez O. and Sánchez F, 1999. *Modelos y cartografía de estimaciones climáticas termopluviométricas para la España peninsula*r. Ministerio de Agricultura, Pesca y Alimentación. Instituto Nacional de Investigación y Tecnología Agraria y Alimentaria. *ISBN: 84-749847-0-X*. 192 p.

Taylor, J.R., 1997. *An Introduction to Error Analysis: The Study of Uncertainties in Physical Measurements*. University Science Books, Sausalito, *CA*. 345 p.

Tveito, O.E., Wegehenkel, M. and Wel, F., 2008. *The use of geographic information systems in Climatology and Meteorology*. *COST Action 719—ESSEM*.

USGS, 1996. *Global 30 Arc-Second Elevation (GTOPO30)*. United States Geological Survery.

Vicente-Serrano, S.M., Saz-Sánchez, M.A., and Cuadrat, J.M., 2003. Comparative analysis of interpolation methods in the middle Ebro Valley (Spain): Application to annual precipitation and temperature. *Climate Research*, 24 (2), 161–180.

Willmott, C.J., 1982. Some comments on the evaluation of model performance. *Bulletin of the American Meteorological Society*, 63 (11), 1309–1313.

FIGURE CAPTIONS

Figure 1. Study area. The map shows the topography of Iberian Peninsula, and the names of the most important spatial units quoted in the text

Figure 2. Spatial distribution of the meteorological stations by altitudinal intervals

Figure 3. Tmax and Tmin Mean Bias Error (MBE) for different elevation bands annual values are shown together January and July

Figure 4. Monthly mean climatology for Tmax

Figure 5. Monthly mean climatology for Tmin

Figure 6. Monthly mean climatology for DTR

Figure 7. Confidence interval (68%) estimated for the LWLR Tmax and Tmin reconstructions for January and July

Tmax	LWLR					RK					RKS				
	MBE	RMSE	MAE	R^2	D	MBE	RMSE	MAE	R^2	D	MBE	RMSE	MAE	R^2	D
January	-0,006	0,823	0,608	0.927	0.981	0,001	0,823	0,605	0.927	0.981	0,002	0,832	0,612	0.925	0.980
Febrary	-0,012	0,814	0,606	0.922	0.979	0,002	0,815	0,608	0.922	0.979	0,002	0,832	0,621	0.919	0.978
March	-0,020	0,860	0,644	0.907	0.975	0,001	0,890	0,667	0.901	0.972	0,002	0,890	0,668	0.901	0.972
April	-0,024	0,913	0,680	0.907	0.975	0,001	0,947	0,706	0.901	0.972	0,001	0,937	0,698	0.903	0.973
May	-0,031	0,978	0,736	0.898	0.972	0,002	1,036	0,775	0.887	0.968	0,000	1,002	0,752	0.894	0.970
June	-0,038	1,100	0,829	0.897	0.972	0,004	1,179	0,876	0.883	0.967	0,000	1,115	0,839	0.895	0.971
July	-0,037	1,163	0,880	0.911	0.976	0,002	1,272	0,946	0.893	0.970	-0,002	1,188	0,895	0.907	0.975
August	-0,040	1,133	0,856	0.906	0.975	0,002	1,223	0,912	0.891	0.970	-0,001	1,157	0,869	0.903	0.973
September	-0,033	0,993	0,747	0.899	0.972	0,000	1,047	0,782	0.888	0.968	-0,001	1,014	0,763	0.895	0.971
October	-0,020	0,863	0,642	0.910	0.976	0,001	0,884	0,657	0.906	0.974	0,003	0,888	0,659	0.905	0.974
November	-0,009	0,823	0,608	0.925	0.980	0,001	0,820	0,604	0.926	0.981	0,000	0,832	0,615	0.924	0.980
December	-0,006	0,839	0,620	0.924	0.980	0,001	0,844	0,620	0.924	0.980	0,002	0,845	0,621	0.924	0.980
Annual	-0,023	0,813	0,612	0.919	0.978	0,001	0,848	0,633	0.904	0.976	0,001	0,844	0,633	0.908	0.977

Table 1. Monthly and anual error model measurements for Tmax.

Tmin	LWLR					RK					RKS				
	MBE	RMSE	MAE	R^2	D	MBE	RMSE	MAE	R^2	D	MBE	RMSE	MAE	R^2	D
January	-0,007	1,020	0,796	0.882	0.968	0,000	1,193	0,936	0.841	0.957	-0,001	1,089	0,864	0.865	0.963
Febrary	-0,009	1,020	0,801	0.883	0.969	-0,001	1,172	0,928	0.848	0.959	-0,001	1,085	0,864	0.868	0.964
March	-0,005	1,024	0,808	0.873	0.965	-0,001	1,148	0,915	0.842	0.957	-0,001	1,085	0,867	0.857	0.961
April	0,003	0,968	0,765	0.880	0.968	-0,002	1,048	0,831	0.861	0.963	-0,004	1,013	0,802	0.869	0.964
May	0,004	1,000	0,785	0.865	0.963	0,001	1,054	0,831	0.850	0.959	-0,002	1,040	0,819	0.854	0.960
June	0,005	1,104	0,856	0.852	0.959	0,003	1,137	0,887	0.844	0.957	0,000	1,141	0,892	0.843	0.957
July	0,005	1,248	0,959	0.844	0.956	0,003	1,291	0,998	0.833	0.954	0,001	1,296	1,004	0.832	0.953
August	0,001	1,256	0,966	0.854	0.960	0,001	1,320	1,025	0.839	0.956	0,000	1,311	1,018	0.841	0.956
September	-0,002	1,178	0,917	0.864	0.963	0,000	1,285	1,011	0.840	0.956	-0,001	1,249	0,984	0.847	0.958
October	-0,004	1,064	0,838	0.879	0.967	-0,001	1,216	0,966	0.845	0.958	-0,001	1,143	0,911	0.861	0.962
November	-0,009	1,031	0,808	0.887	0.970	0,000	1,215	0,956	0.846	0.958	0,001	1,109	0,881	0.869	0.964
December	-0,005	1,018	0,791	0.885	0.969	-0,001	1,199	0,937	0.844	0.958	0,000	1,089	0,859	0.869	0.964
Annual	-0,002	1,011	0,797	0.877	0.967	-0,001	1,130	0,899	0.844	0.960	-0,002	1,078	0,860	0.856	0.962

Table 2. Monthly and anual error model measurements for Tmin.

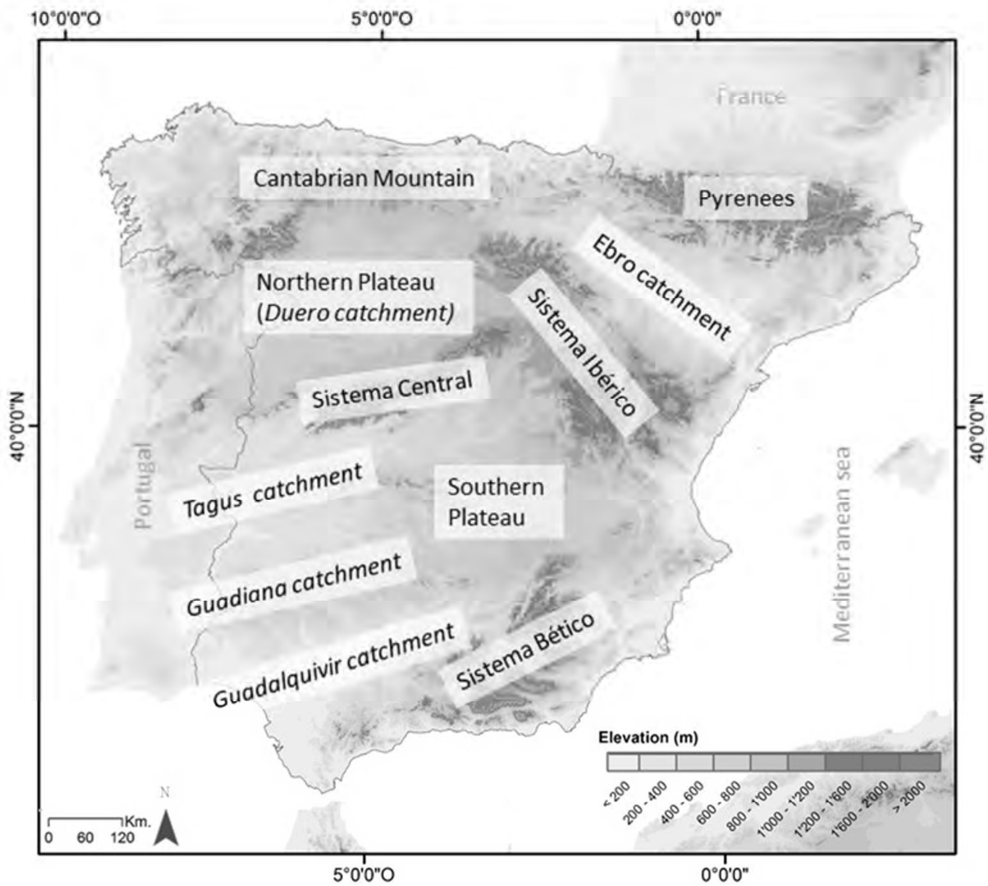

Study area. The map shows the topography of Iberian Peninsula, and the names of the most important spatial units quoted in the text

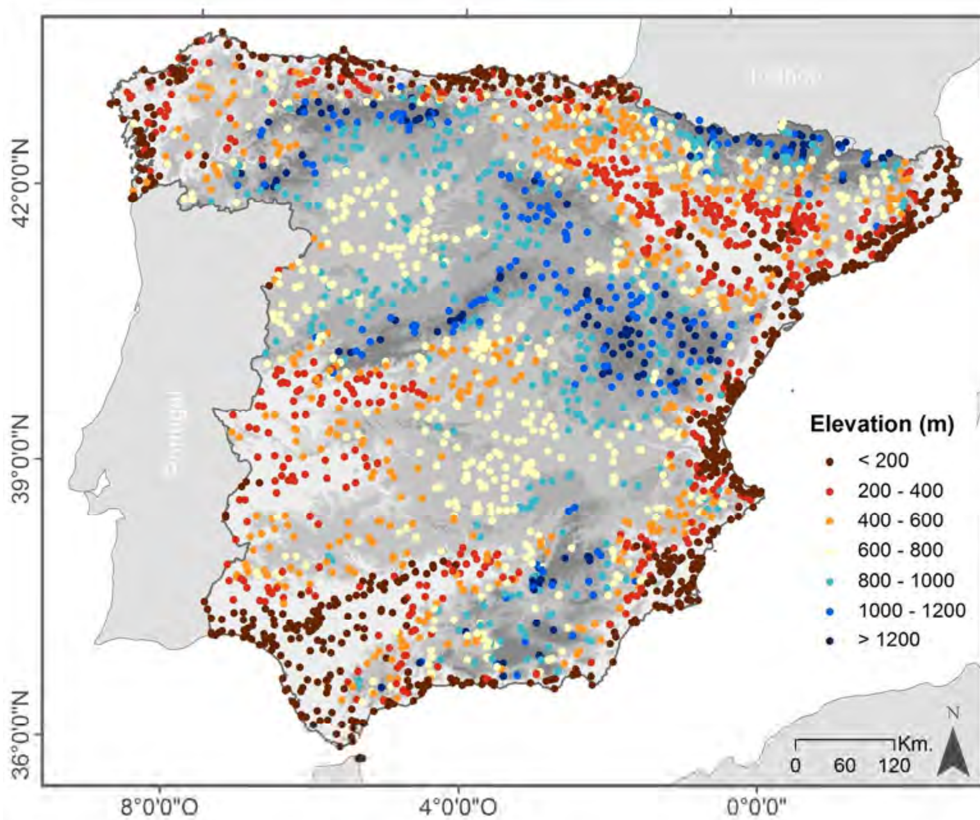

Spatial distribution of the meteorological stations by altitudinal intervals

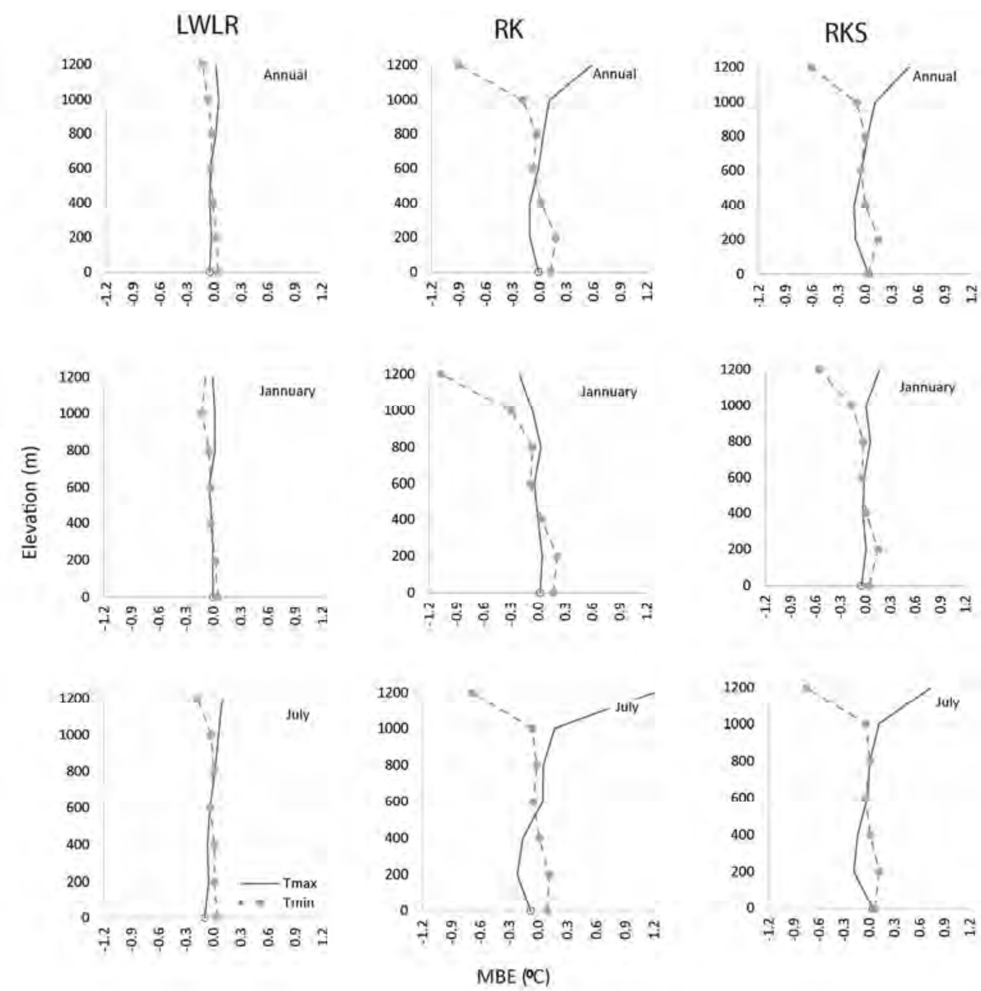

Tmax and Tmin Mean Biass Error (MBE) for different elevation bands annual values are shown together January and July
965x951mm (72 x 72 DPI)

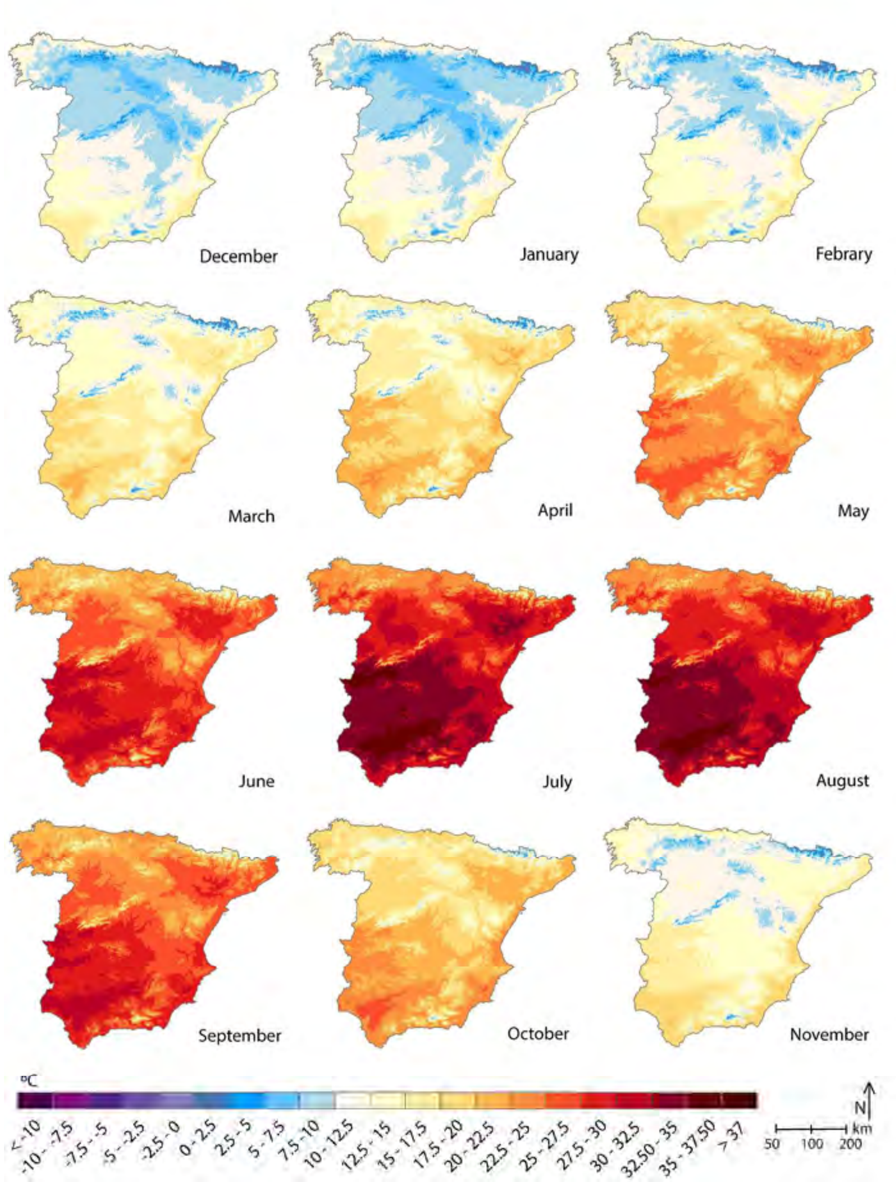

Monthly mean climatology for Tmax
282x375mm (300 x 300 DPI)

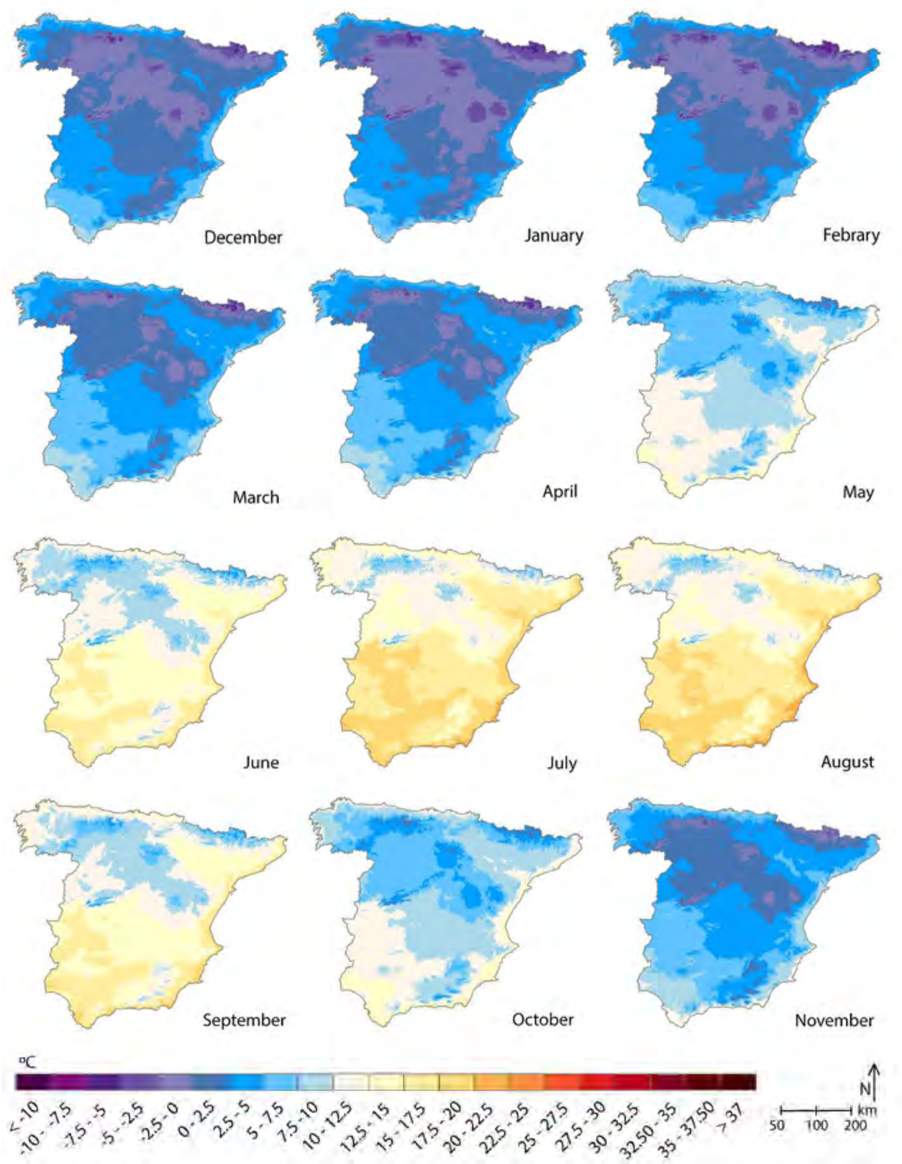

Monthly mean climatology for Tmin
282x373mm (300 x 300 DPI)

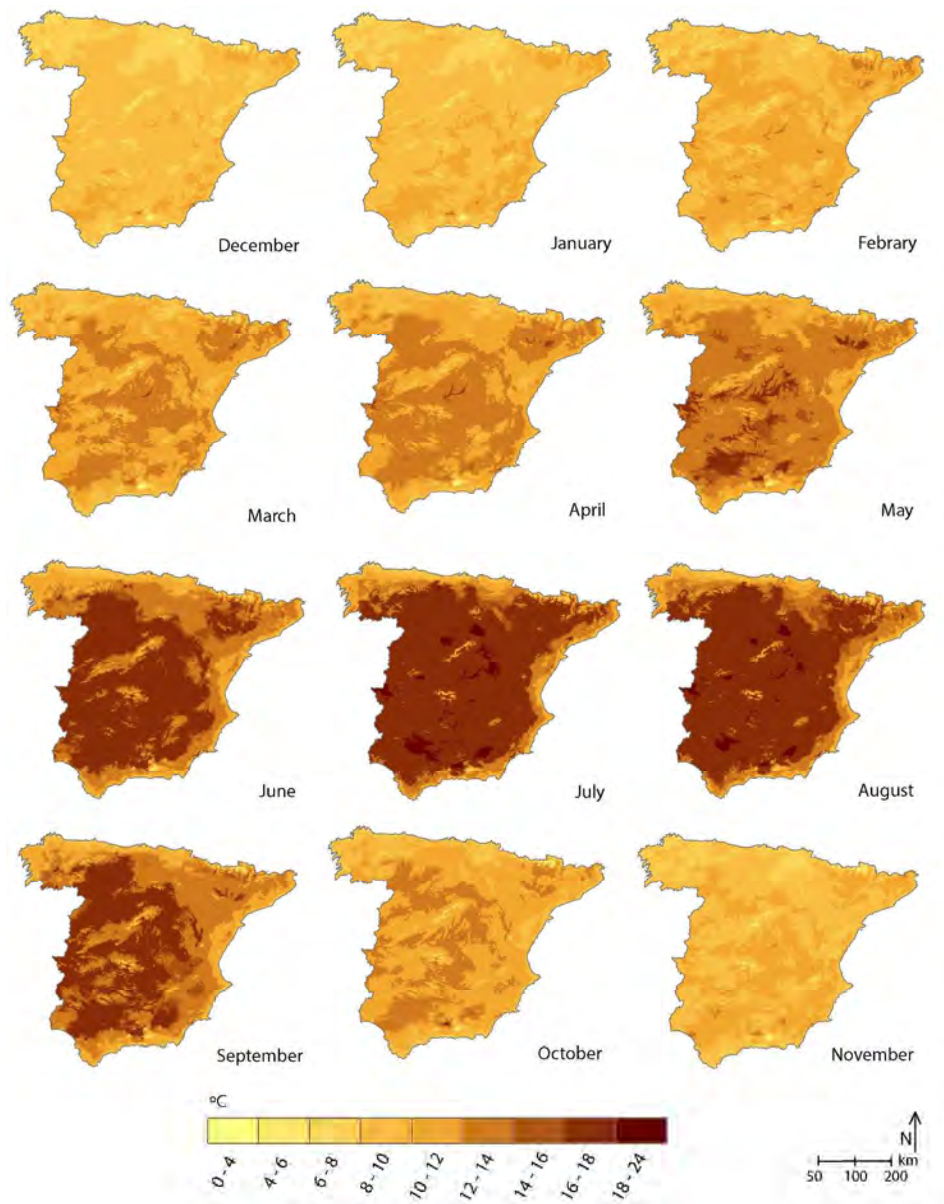

Monthly mean climatology for DTR
214x271mm (300 x 300 DPI)

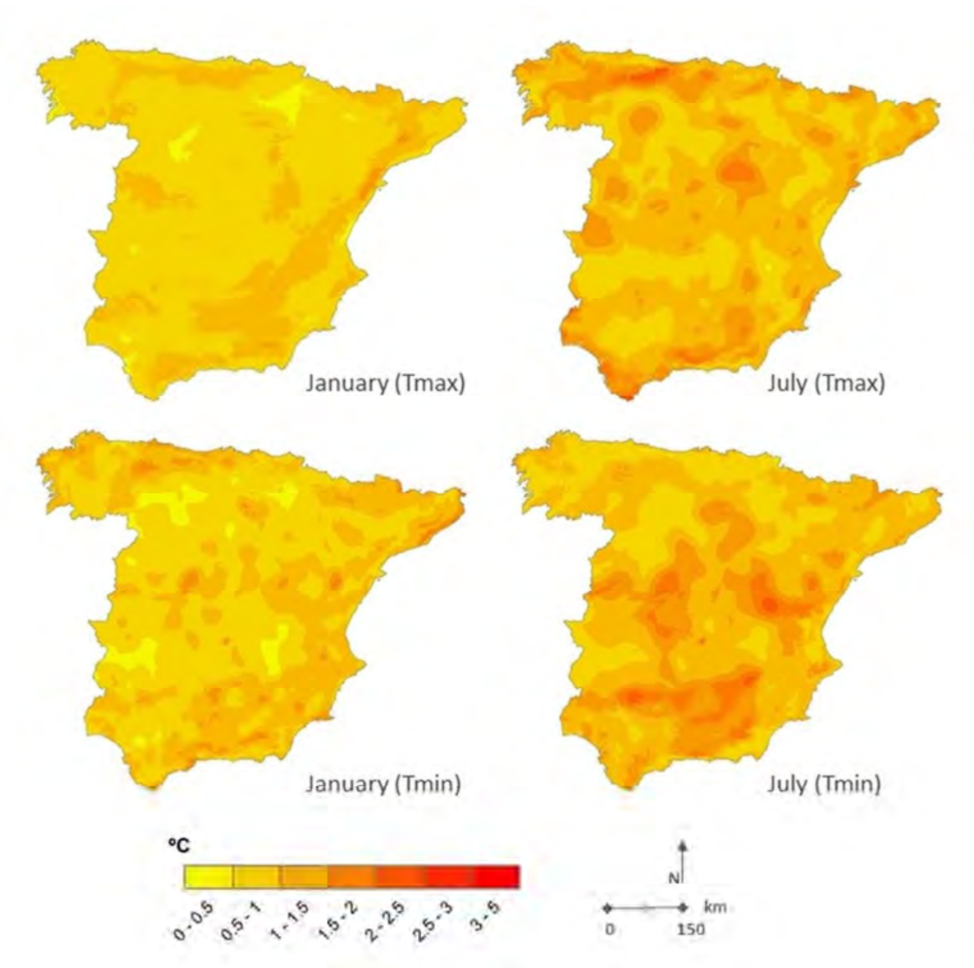

Confidence interval (68%) estimated for the LWLR Tmax and Tmin reconstructions for January and July